Temperature-dependent refractive index measurements of CaF_2, Suprasil 3001, and S-FTM16 for the Euclid Near Infrared Spectrometer and Photometer

[a]Douglas B. Leviton, [b]Kevin H. Miller, [b]Manuel A. Quijada, [c]Frank D. Grupp

[a]Leviton Metrology Solutions, Inc., Boulder, CO 80301
[b]NASA Goddard Space Flight Center, Greenbelt, MD 20771
[c]Max Planck Institut for extraterrestrial Physics, Garching near Munich 85748

ABSTRACT

Using the Cryogenic High Accuracy Refraction Measuring System (CHARMS) at NASA's Goddard Space Flight Center, we measured absolute refractive indices at temperatures from 100 to 310 K at wavelengths from 0.42 to 3.6 microns for CaF_2, Suprasil 3001 fused silica, and S-FTM16 glass in support of lens designs for the Near Infrared Spectrometer and Photometer (NISP) for ESA's Euclid dark energy mission. We report absolute refractive index, dispersion ($dn/d\lambda$), and thermo-optic coefficient (dn/dT) for these materials. In this study, materials from different melts were procured to understand index variability in each material. We provide temperature-dependent Sellmeier coefficients based on our data to allow accurate interpolation of index to other wavelengths and temperatures. For calcium fluoride (CaF_2) and S-FTM16, we compare our current measurements with CHARMS measurements of these materials made in the recent past for other programs. We also compare Suprasil 3001's indices to those of other forms of fused silica we have measured in CHARMS.

Keywords: calcium fluoride, Suprasil 3001, S-FTM16, CHARMS, Euclid, NISP, cryogenic refractive index, temperature-dependent, dispersion, thermo-optic coefficient, infrared

1. INTRODUCTION

The Cryogenic High Accuracy Refraction Measuring System (CHARMS) was developed at the NASA Goddard Space Flight Center (GSFC) to measure absolute refractive index (in vacuum) down to temperatures as low as 15 K with unsurpassed accuracy using minimum deviation refractometry.[1-3] Initially, CHARMS was developed in support of the optical design for James Webb Space Telescope's (JWST) Near Infrared Camera (NIRCam)[4] with an eye towards cryogenic refractive index measurements for a wide variety of infrared materials to serve the entire scientific community, both space-based and ground-based. To that end, CHARMS has supported a wide variety of international programs including JWST, the Keck Multi-Object Spectrometer for Infra-Red Exploration (MOSFIRE)[5], the ESO UT1 CRyogenic high-resolution InfraRed Echelle Spectrograph (CRIRES)[6] and VLT K-band Multi-Object Spectrograph (KMOS)[7] and X-shooter near IR spectrograph[8], the GMT Near Infrared Multi-Object Spectrograph (NIRMOS)[9], the Euclid Near Infrared Spectrometer and Photometer (NISP)[10,11], NASA's Transiting Exoplanet Survey Satellite (TESS)[12] and Wide Field Infrared Survey Telescope (WFIRST)[13], and the CHARIS high contrast imaging spectrograph for the Subaru telescope.[14,15] CHARMS has now been used for measurements at wavelengths as low as 0.35 μm in the near UV and to temperatures as high as 335 K (62 C). Figure 1 is a photograph of CHARMS at GSFC.

For the present study, we used CHARMS to measure absolute refractive indices for lens materials for Euclid's NISP instrument, namely calcium fluoride (CaF_2), Ohara S-FTM16 glass, and Heraeus Suprasil 3001, a low hydroxyl ion content form of synthetic fused silica with suppressed absorption out to 3.0 μm in the IR. A main purpose of this study was to evaluate batch-to-batch index variability to characterize the batches of materials purchased to build NISP's lenses and to improve the tolerancing process in the NISP optical design, among other things. Table 1 summarizes batch information for each material, prism ID's, and apex angles along with wavelength and temperature ranges covered in CHARMS measurements.

* author contact: doug@levitonmetrology.com, 240-478-7877

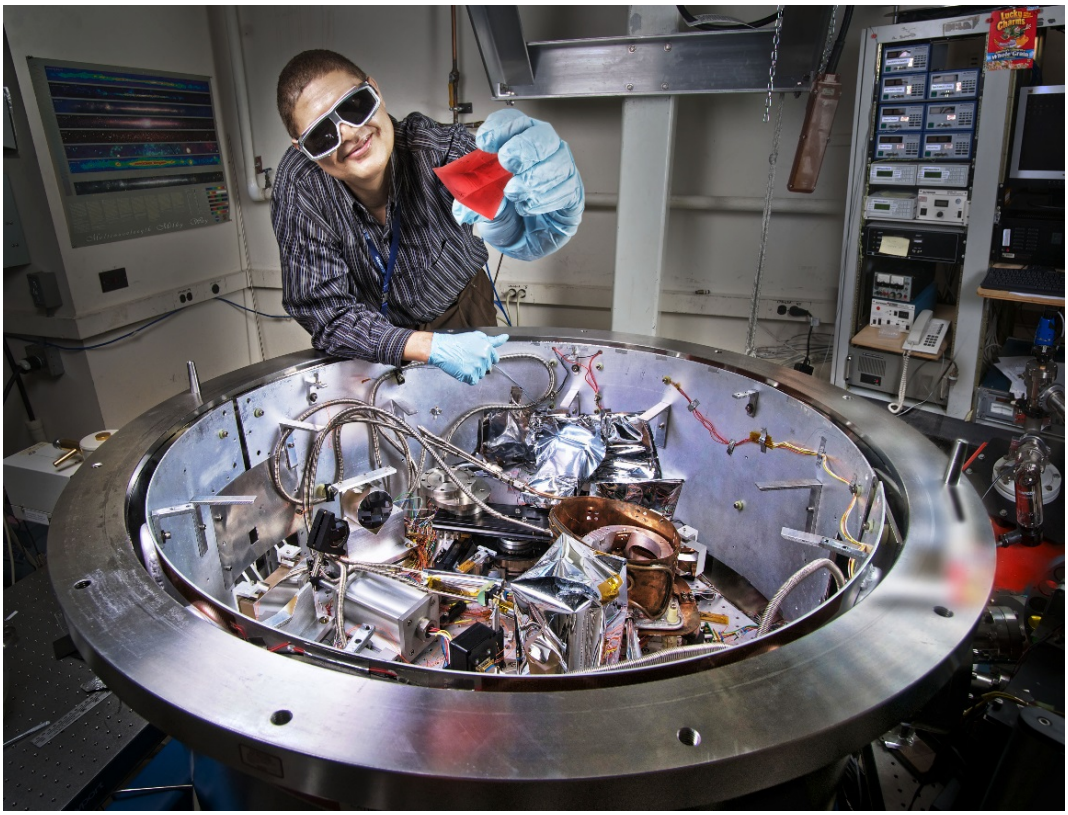

Figure 1 – CHARMS high accuracy, cryogenic refractometer at NASA GSFC (photo by Bert Pasquale and Scott Smith/GSFC)

Table 1 – summary of batch information and CHARMS wavelength and temperature coverage for each NISP material; apex angles α are measured to an accuracy better than 0.5 arcseconds

Heraeus Suprasil 3001	Ohara S-FTM16	CaF2
0.416 μm ≤ λ ≤ 3.16 μm; 110 K ≤ T ≤ 310 K	0.416 μm ≤ λ ≤ 2.72 μm; 110 K ≤ T ≤ 310 K	0.416 μm ≤ λ ≤ 3.56 μm; 100 K ≤ T ≤ 310 K
SN1, Melt 1, No. 1, α = 58.95916°	SN1 - Melt 1, α = 59.02502°	SN1, α = 53.98244°
SN4, Melt 1, No.2, α = 58.95767°	SN3 - Melt 1, α = 59.01451°	SN2, α = 53.98423°
SN6, Melt 1, No.3, α = 58.99970°	SN4 - Melt 1, α = 59.02539°	SN3, α = 54.01943°
SN7, Melt 2, No. 1, α = 58.98341°	SN7 - Melt 2, α = 58.95732°	
SN9, Melt 2, No. 2, α = 58.99343°	SN8 - Melt 2, α = 58.98977°	
SN2, Melt 2, No. 3, α = 59.02609°	SN11 - Melt 2, α = 58.99634°	

2. PRESENTATION OF MEASURED INDEX DATA

Detailed descriptions of our data acquisition and reduction processes are documented elsewhere[16], as is our calibration strategy[1]. We fit our raw, measured index data to a temperature dependent Sellmeier model of the form:

$$n^2(\lambda,T) - 1 = \sum_{i=1}^{m} \frac{S_i(T)\cdot\lambda^2}{\lambda^2 - \lambda_i^2(T)} \quad ,$$

where S_i are theoretical strengths of resonance features in the material at wavelengths λ_i . When dealing with a wavelength interval between wavelengths of physical resonances in a material, the summation may be approximated by typically only three terms (m=3).[17] With this approximation, resonance strengths S_i and wavelengths λ_i have no physical significance but are simply parameters used to generate adequately accurate fits to measured data. If these parameters are assumed to be functions of temperature, T, one can generate a temperature-dependent Sellmeier model for n(λ,T).

Historically, this modeling approach has enjoyed significant success for a variety of materials despite a rather serious sparseness of available index data to cover a wide range of temperatures and wavelengths upon which to base a model. Sadly, some designers have experienced disappointing performance in as-built lenses by extrapolating outside the ranges of applicability of published Sellmeier models. One solution to lacking measured index data has been to appeal to room temperature refractive index data at several wavelengths to anchor a model and then to extrapolate index values for other temperatures using accurate measurements of the thermo-optic coefficient at those temperatures which are much easier to make than accurate measurements of the index itself at exotic temperatures. Such extrapolation can be potentially dangerous, depending on the sample material in question and the required accuracy of index knowledge.

Meanwhile, with CHARMS, we directly measure index itself, densely sampling over a wide range of wavelengths and temperatures to produce a model with residuals on the order of (usually significantly less than) the uncertainties in our raw index measurements. For models for the NISP materials, we found that 3rd order temperature dependencies in all three terms in each of S_i and λ_i are adequate. The Sellmeier equation consequently becomes:

$$n^2(\lambda,T)-1 = \sum_{i=1}^{3}\frac{S_i(T)\cdot\lambda^2}{\lambda^2-\lambda_i^2(T)} \qquad \text{where,}$$

$$S_i(T) = \sum_{j=0}^{3} S_{ij}\cdot T^j$$

$$\lambda_i(T) = \sum_{j=0}^{3} \lambda_{ij}\cdot T^j$$

The Sellmeier model is our best statistical representation of the raw, measured index data over the complete measured ranges of wavelength and temperature and allows accurate computation of the derivatives of index with respect to those two parameters. All tabulated values for refractive index and its derivatives have been calculated using the Sellmeier coefficients found later in Section 4. Typically, measured index values agree with the fits to less than our measurement uncertainties found in Section 3. Three things to remember when applying these Sellmeier fits and coefficients: 1) do not attempt to apply the fit outside the stated range of applicability; 2) test the fits to assure you can reproduce any value in Tables 5, 6, and 7; and 3) make sure to use all significant figures listed for each coefficient.

3. MEASUREMENT UNCERTAINTIES

CHARMS was designed specifically to minimize all sources of systematic errors in refractive index measurement and to provide measurements of highest achievable precision at both ambient and cryogenic temperatures. A non-exhaustive discussion which touches on the four most significant possible contributors to index errors has been published earlier.[21] As refractive index is a function of wavelength and temperature, likewise so is index measurement uncertainty.

Tables 2, 3, and 4 summarize estimated uncertainties for single index measurements for Suprasil 3001, S-FTM16, and CaF_2, respectively. Figure 2 contains surface plots of these uncertainty values. These plots are distinctly different for each of these types of materials. Glasses which are good insulators (low thermal conductivity) tend to sustain higher temperature gradients at low temperatures such that knowledge of temperature of the part of the sample through which refracted light passes is less good. With short wavelength cutoffs near 350 nm, dispersion in the blue is relatively high. Thus, index uncertainty trends upward at low temperatures and short wavelengths at the same time. For good insulators with deep or far UV short wavelength cutoffs like fused quartz materials such as Suprasil 3001, dispersion in the blue is relatively low, so index uncertainty trends upwards mostly due to temperature uncertainty at low temperatures and not so much due to higher dispersion. For crystalline materials like CaF2 which have higher thermal conductivity, temperature gradients in the sample are low and knowledge of temperature at low temperatures is better. With a very short cutoff wavelength and low dispersion in the blue, CaF_2's uncertainty plot is relatively low and flat. The slight increase in uncertainty above 1 μm for CaF_2 is due to slightly lower certainty in measuring beam deviations in the IR using a slit scan method with the IR detector versus scanning the slit image across a CCD image sensor for the visible and near IR.

Table 2 – Uncertainty of absolute refractive index of Suprasil 3001 in CHARMS for selected wavelengths & temperatures

wavelength	120 K	150 K	200 K	250 K	300 K
0.45 µm	3.6E-05	2.2E-05	2.2E-05	1.7E-05	1.2E-05
0.65 µm	3.1E-05	1.8E-05	1.8E-05	1.3E-05	8.4E-06
1.00 µm	3.0E-05	1.7E-05	1.7E-05	1.2E-05	7.6E-06
2.00 µm	3.2E-05	1.9E-05	1.9E-05	1.4E-05	1.0E-05
3.00 µm	3.2E-05	2.0E-05	2.0E-05	1.4E-05	1.0E-05

Table 3 – Uncertainty of absolute refractive index of S-FTM16 in CHARMS for selected wavelengths & temperatures

wavelength	110 K	150 K	200 K	250 K	300 K
0.45 µm	2.6E-05	2.5E-05	2.3E-05	2.1E-05	2.1E-05
0.65 µm	1.3E-05	1.2E-05	1.0E-05	7.9E-06	7.0E-06
1.00 µm	1.0E-05	8.7E-06	7.1E-06	4.8E-06	3.7E-06
1.80 µm	9.9E-06	8.3E-06	6.6E-06	4.5E-06	3.3E-06
2.60 µm	9.6E-06	8.3E-06	6.6E-06	3.3E-06	3.5E-06

Table 4 – Uncertainty of absolute refractive index of CaF_2 in CHARMS for selected wavelengths & temperatures

wavelength	110 K	150 K	200 K	250 K	300 K
0.45 µm	7.1E-06	8.0E-06	8.3E-06	8.5E-06	8.2E-06
0.63 µm	6.1E-06	7.0E-06	7.3E-06	7.7E-06	7.4E-06
1.00 µm	5.8E-06	6.7E-06	7.0E-06	7.4E-06	7.0E-06
2.20 µm	8.6E-06	9.5E-06	9.8E-06	1.0E-05	9.9E-06
3.40 µm	8.6E-06	9.4E-06	9.8E-06	7.5E-06	9.7E-06

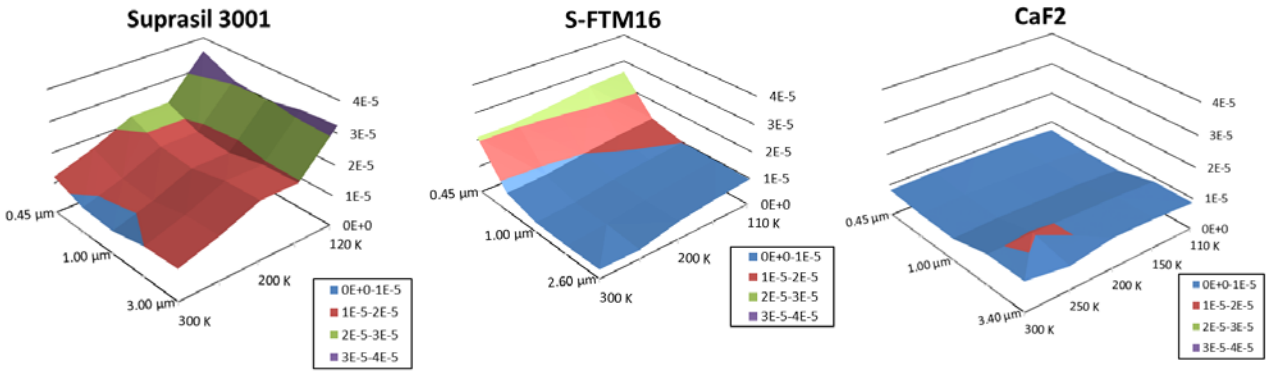

Figure 2 – Surface plots of uncertainties for single index measurements of Suprasil 3001, S-FTM16, and CaF_2 in CHARMS with wavelength and temperature

4. MEASUREMENT RESULTS

The coefficients for temperature-dependent Sellmeier fits of measured index to wavelength and temperature (to be used as prescribed in Section 3) for Suprasil 3001, S-FTM16, and CaF_2 are listed in Tables 5, 6, and 7, respectively. The number of individual index measurements involved in each fit is listed in each table's legend along with the average absolute fit residuals and ranges of wavelength and temperature applicability for each fit. Note: the sensitivity of index accuracy when using the fit to the number of significant digits listed for each coefficient is unknown, so at least eight significant digits are reported for all coefficients (very likely more than needed).

For Suprasil 3001, the two melts measured were indistinguishable to within our measurement uncertainties, so all measured indices contributed to the single fit in Table 5. The same was true for S-FTM16 (Table 6). For CaF_2, there

was a barely discernable difference between the three batches compared to our index uncertainties. On balance, over all measured wavelengths and temperatures, prism SN2 had higher index than SN3 by 4.7E-6, and SN3 had higher index than SN1 by 1.0 E-5. Wavelength and temperature derivatives are the same for all three batches of CaF_2, so one combined fit is represented in Table 7. Average absolute fit residuals for each batch taken separately were very low: SN1 – 3.2E-6; SN2 – 2.5E-6; and SN3 – 2.8E-6.

Table 5 – Coefficients for temperature-dependent Sellmeier fit of absolute refractive index of Suprasil 3001

Coefficients for temperature-dependent Sellmeier equation for Suprasil 3001; application: 110 K ≤ T ≤ 310 K; 0.416 µm ≤ λ ≤ 3.16 µm Average absolute fit residual = 6.2E-6; fit based on 5,960 individual index measurements						
	S_1	**S_2**	**S_3**	**λ_1**	**λ_2**	**λ_3**
Constant term	2.0949611E-01	8.9235769E-01	8.7663249E-01	-5.8714652E-02	9.7313583E-02	9.8137923E+00
T term	2.7399685E-04	-2.7192212E-04	3.0330081E-04	9.2480992E-04	6.2387297E-05	1.5530010E-03
T^2 term	1.4069372E-06	-1.3618554E-06	-1.6082403E-06	-2.6028270E-06	-3.0113200E-07	-8.3011284E-06
T^3 term	7.6027567E-09	-7.6204300E-09	2.6861660E-09	2.9960201E-09	8.8515242E-10	1.3964033E-08

Table 6 – Coefficients for temperature-dependent Sellmeier fit of absolute refractive index of S-FTM16

Coefficients for temperature-dependent Sellmeier equation for S-FTM16; application: 110 K ≤ T ≤ 310 K; 0.416 µm ≤ λ ≤ 2.72 µm Average absolute fit residual = 8.0E-6; fit based on 7,312 individual index measurements						
	S_1	**S_2**	**S_3**	**λ_1**	**λ_2**	**λ_3**
Constant term	1.2150563E+00	2.6092274E-01	9.1036236E-01	8.8057716E-02	2.1069351E-01	9.9088653E+00
T term	1.3688149E-03	-1.3777543E-03	5.2376973E-03	1.3971543E-04	3.3594857E-04	2.3036544E-02
T^2 term	-6.0124208E-06	5.9765687E-06	-2.9744085E-05	-5.8573252E-07	-1.4632989E-06	-1.3022470E-04
T^3 term	8.0442131E-09	-7.9534661E-09	5.1610493E-08	7.5117193E-10	2.0146446E-09	2.2620436E-07

Table 7 – Coefficients for temperature-dependent Sellmeier fit of absolute refractive index of CaF_2

Coefficients for temperature-dependent Sellmeier equation for CaF_2; application: 100 K ≤ T ≤ 310 K; 0.416 µm ≤ λ ≤ 3.56 µm Average absolute fit residual = 6.3E-6; fit based on 4,600 individual index measurements						
	S_1	**S_2**	**S_3**	**λ_1**	**λ_2**	**λ_3**
Constant term	9.64897439E-01	8.04911323E-02	2.24550341E+00	-6.61856475E-02	1.40131234E-01	2.72931138E+01
T term	-7.38704087E-04	7.44817508E-04	3.13937373E-02	-1.21180637E-05	-2.42570135E-04	1.40040106E-01
T^2 term	7.17518006E-07	-8.40049522E-07	-1.67438455E-04	2.21072817E-07	9.31841153E-07	-7.43081369E-04
T^3 term	1.09741437E-09	-9.71236119E-10	2.58329027E-07	-5.27928096E-10	-1.29845516E-09	1.14612930E-06

Tables 8, 9, and 10 contain absolute refractive indices of Suprasil 3001 computed from its Sellmeier fit along with its wavelength and temperature derivatives – spectral dispersion, $dn/d\lambda$, and thermo-optic coefficient, dn/dT, respectively. Figures 3 is a graph of Suprasil 3001's spectral index while Figure 4 contains graphs of its dispersion and thermo-optic coefficient.

Tables 11, 12, and 13 contain absolute refractive indices of S-FTM16 computed from its Sellmeier fit along with spectral dispersion and thermo-optic coefficient, respectively. Figures 5 is a graph of S-FTM16's spectral index while Figure 6 contains graphs of its dispersion and thermo-optic coefficient.

Tables 14, 15, and 16 contain absolute refractive indices of CaF_2 computed from its Sellmeier fit along with spectral dispersion and thermo-optic coefficient, respectively. Figures 7 is a graph of CaF_2's spectral index while Figure 8 contains graphs of its dispersion and thermo-optic coefficient.

Table 8 – Computed absolute refractive index of Suprasil 3001 for selected wavelengths and temperatures

wavelength [μm]	110 K	150 K	200 K	250 K	300 K
0.416	1.467834	1.468036	1.468360	1.468753	1.469207
0.50	1.461730	1.461925	1.462236	1.462611	1.463044
0.65	1.455976	1.456164	1.456463	1.456823	1.457239
0.8	1.452778	1.452962	1.453255	1.453608	1.454017
1.0	1.449894	1.450076	1.450365	1.450713	1.451117
1.5	1.444125	1.444305	1.444589	1.444934	1.445334
2.0	1.437625	1.437804	1.438089	1.438433	1.438834
3.2	1.413933	1.414115	1.414400	1.414749	1.415160

Table 9 – Dispersion in Suprasil 3001 for selected wavelengths and temperatures (units 1/μm)

wavelength [μm]	110 K	150 K	200 K	250 K	300 K
0.45	-0.0727	-0.0728	-0.0729	-0.0731	-0.0734
0.50	-0.0562	-0.0562	-0.0564	-0.0565	-0.0567
0.65	-0.0273	-0.0273	-0.0274	-0.0274	-0.0275
0.8	-0.0173	-0.0173	-0.0173	-0.0174	-0.0174
1.0	-0.0126	-0.0126	-0.0126	-0.0126	-0.0126
1.5	-0.0117	-0.0117	-0.0117	-0.0118	-0.0118
2.0	-0.0149	-0.0149	-0.0149	-0.0149	-0.0149
3.0	-0.0236	-0.0236	-0.0236	-0.0236	-0.0236

Table 10 – Thermo-optic coefficient (dn/dT) of Suprasil 3001 for selected wavelengths and temperatures (units 1/K)

wavelength [μm]	120 K	150 K	200 K	250 K	300 K
0.42	4.6E-06	5.8E-06	7.2E-06	8.5E-06	9.7E-06
0.50	4.5E-06	5.5E-06	6.9E-06	8.1E-06	9.3E-06
0.65	4.4E-06	5.3E-06	6.6E-06	7.8E-06	8.9E-06
0.8	4.3E-06	5.2E-06	6.5E-06	7.6E-06	8.7E-06
1.0	4.2E-06	5.1E-06	6.4E-06	7.5E-06	8.6E-06
1.5	4.2E-06	5.1E-06	6.3E-06	7.5E-06	8.5E-06
2.0	4.2E-06	5.0E-06	6.3E-06	7.5E-06	8.5E-06
3.2	4.3E-06	5.1E-06	6.3E-06	7.6E-06	8.9E-06

Table 11 – Computed absolute refractive index of S-FTM16 for selected wavelengths and temperatures

wavelength [μm]	110 K	150 K	200 K	250 K	300 K
0.416	1.620608	1.620506	1.620413	1.620389	1.620432
0.50	1.603403	1.603265	1.603124	1.603036	1.602999
0.65	1.589232	1.589079	1.588907	1.588775	1.588689
0.8	1.582375	1.582215	1.582033	1.581884	1.581780
1.0	1.577111	1.576948	1.576759	1.576602	1.576488
1.5	1.569221	1.569055	1.568866	1.568707	1.568585
2.0	1.562217	1.562054	1.561869	1.561716	1.561596
2.6	1.552224	1.552068	1.551890	1.551746	1.551643

Table 12 – Dispersion in S-FTM16 for selected wavelengths and temperatures (units 1/μm)

wavelength [μm]	110 K	150 K	200 K	250 K	300 K
0.45	-0.2048	-0.2052	-0.2058	-0.2066	-0.2075
0.50	-0.1493	-0.1495	-0.1499	-0.1504	-0.1510
0.65	-0.0623	-0.0624	-0.0625	-0.0627	-0.0629
0.8	-0.0345	-0.0345	-0.0346	-0.0347	-0.0347
1.0	-0.0208	-0.0208	-0.0208	-0.0209	-0.0209
1.5	-0.0137	-0.0137	-0.0137	-0.0137	-0.0137
2.0	-0.0151	-0.0151	-0.0151	-0.0151	-0.0151
2.6	-0.0188	-0.0188	-0.0187	-0.0187	-0.0187

Table 13 – Thermo-optic coefficient (dn/dT) of S-FTM16 for selected wavelengths and temperatures (units 1/K)

wavelength [μm]	110 K	150 K	200 K	250 K	290 K
0.42	-2.4E-06	-2.3E-06	-8.5E-07	4.0E-07	1.3E-06
0.50	-3.4E-06	-3.1E-06	-2.1E-06	-1.1E-06	-3.9E-07
0.65	-3.8E-06	-3.6E-06	-2.9E-06	-2.0E-06	-1.4E-06
0.8	-4.0E-06	-3.8E-06	-3.2E-06	-2.4E-06	-1.8E-06
1.0	-4.1E-06	-3.9E-06	-3.4E-06	-2.6E-06	-2.0E-06
1.5	-4.2E-06	-3.9E-06	-3.4E-06	-2.7E-06	-2.2E-06
2.0	-4.1E-06	-3.9E-06	-3.3E-06	-2.6E-06	-2.1E-06
2.8	-3.8E-06	-3.7E-06	-3.1E-06	-2.2E-06	-1.5E-06

Table 14 – Computed absolute refractive index of CaF_2 for selected wavelengths and temperatures

wavelength [µm]	100 K	150 K	200 K	250 K	300 K
0.416	1.442750	1.442457	1.442041	1.441560	1.441027
0.50	1.438549	1.438247	1.437824	1.437330	1.436789
0.65	1.434681	1.434371	1.433941	1.433437	1.432885
0.8	1.432660	1.432346	1.431914	1.431405	1.430849
1.0	1.431024	1.430708	1.430274	1.429763	1.429204
1.5	1.428402	1.428086	1.427652	1.427141	1.426581
2.0	1.425988	1.425675	1.425242	1.424735	1.424179
3.6	1.415262	1.414972	1.414549	1.414061	1.413527

Table 15 – Dispersion in CaF_2 for selected wavelengths and temperatures (units 1/µm)

wavelength [µm]	100 K	150 K	200 K	250 K	300 K
0.45	-0.05001	-0.05011	-0.05021	-0.05035	-0.05046
0.50	-0.03841	-0.03850	-0.03856	-0.03868	-0.03876
0.65	-0.01784	-0.01788	-0.01791	-0.01795	-0.01800
0.8	-0.01044	-0.01046	-0.01047	-0.01050	-0.01052
1.0	-0.00664	-0.00664	-0.00665	-0.00665	-0.00666
1.5	-0.00470	-0.00470	-0.00470	-0.00469	-0.00469
2.0	-0.00519	-0.00518	-0.00518	-0.00517	-0.00516
3.4	-0.00803	-0.00801	-0.00800	-0.00799	-0.00797

Table 16 – Thermo-optic coefficient (dn/dT) of CaF_2 for selected wavelengths and temperatures (units 1/K)

wavelength [µm]	110 K	150 K	200 K	250 K	300 K
0.42	-4.8E-06	-7.4E-06	-9.0E-06	-1.0E-05	-1.1E-05
0.50	-5.0E-06	-7.5E-06	-9.3E-06	-1.0E-05	-1.1E-05
0.65	-5.3E-06	-7.6E-06	-9.4E-06	-1.1E-05	-1.1E-05
0.8	-5.4E-06	-7.6E-06	-9.5E-06	-1.1E-05	-1.1E-05
1.0	-5.5E-06	-7.6E-06	-9.6E-06	-1.1E-05	-1.1E-05
1.5	-5.5E-06	-7.6E-06	-9.6E-06	-1.1E-05	-1.2E-05
2.0	-5.4E-06	-7.6E-06	-9.5E-06	-1.1E-05	-1.2E-05
3.6	-4.8E-06	-7.4E-06	-9.3E-06	-1.0E-05	-1.1E-05

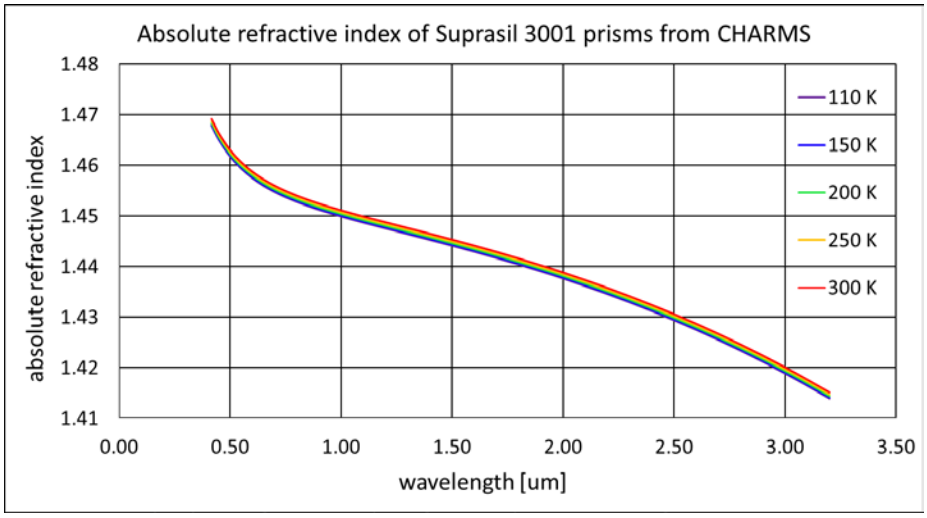

Figure 3 –Absolute spectral refractive index n of Suprasil 3001 for selected temperatures

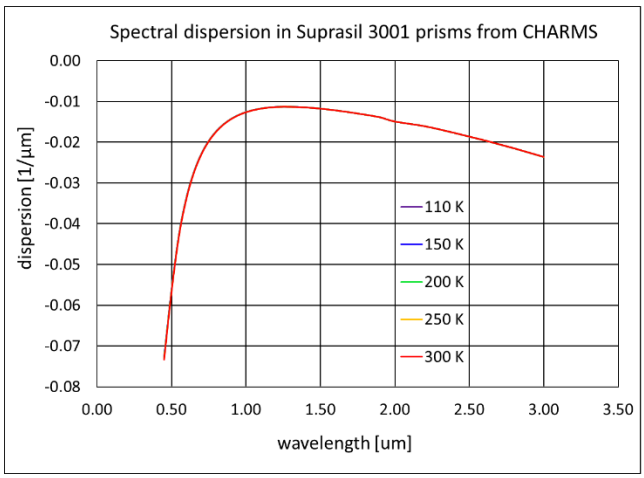

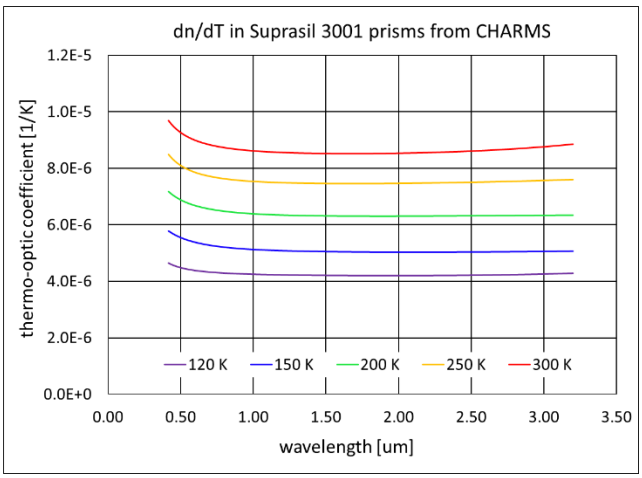

Figure 4 – left) Spectral dispersion (dn/dλ); right) thermo-optic coefficient (dn/dT) of Suprasil 3001 for selected temperatures

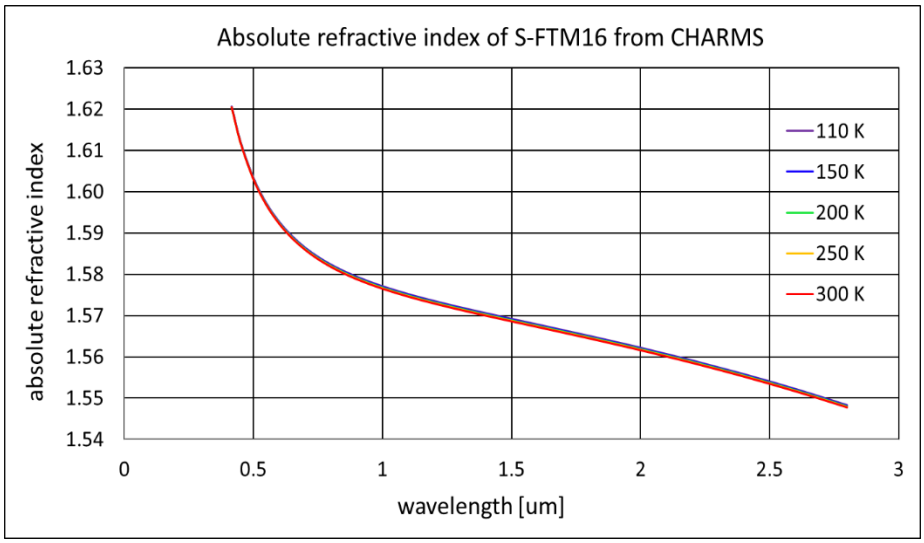

Figure 5 –Absolute spectral refractive index n of S-FTM16 for selected temperatures

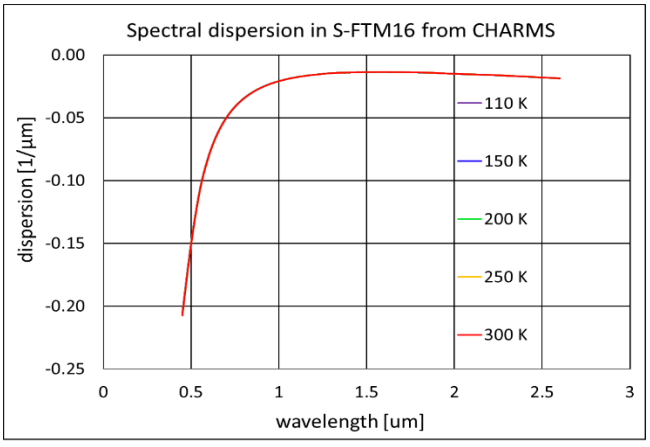

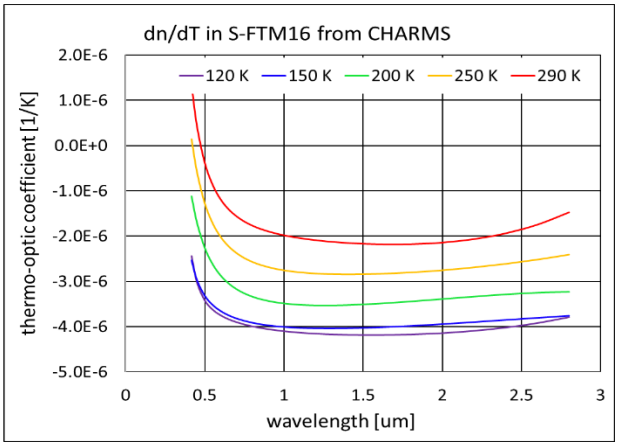

Figure 6 – left) Spectral dispersion (dn/dλ); right) thermo-optic coefficient (dn/dT) of S-FTM16 for selected temperatures

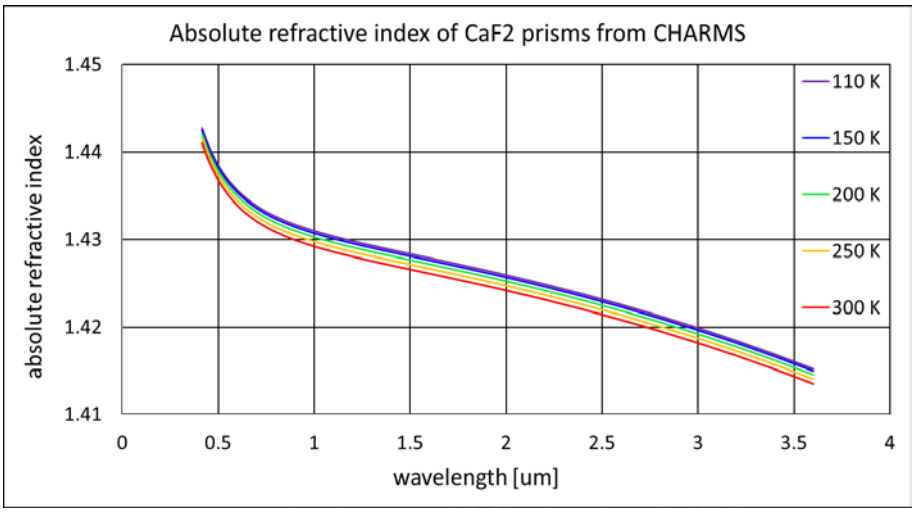

Figure 7 –Absolute spectral refractive index n of CaF_2 for selected temperatures

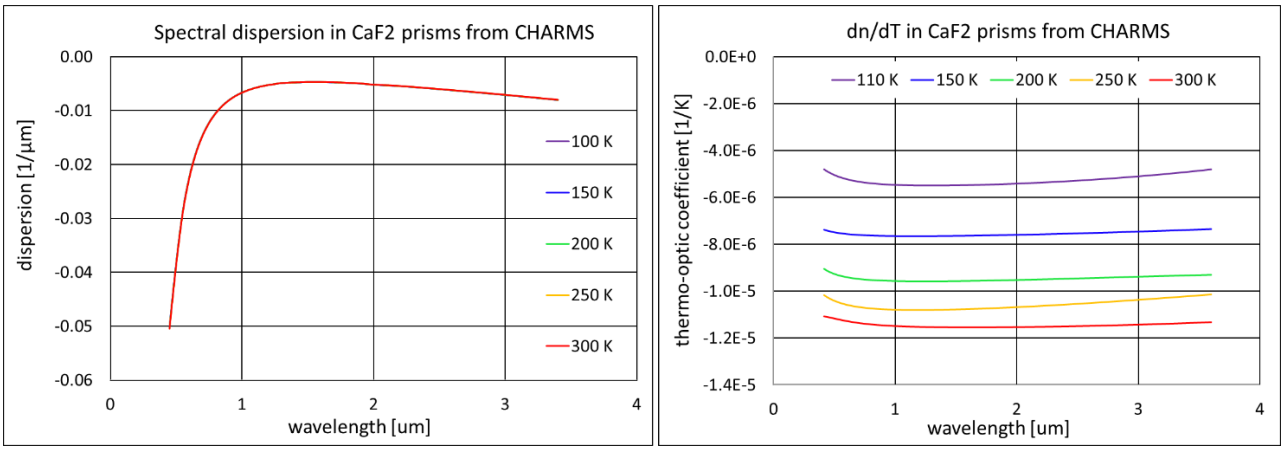

Figure 8 – left) Spectral dispersion (dn/dλ); right) thermo-optic coefficient (dn/dT) of CaF_2 for selected temperatures

5. COMPARISON WITH PAST STUDIES

5.1 Suprasil 3001

While we know of no previous studies of Suprasil 3001 at cryogenic temperatures, we have measured refractive index of three other kinds of synthetic fused silica which makes for an interesting comparison as fused silica is often thought of as "if you've seen one, you've seen them all" material. In Figure 9, we compare our measurements with 1) the catalog room temperature (293 K or 20 C) dispersion relation for the "Suprasil family"[18] ; 2) the catalog room temperature dispersion relation for Homosil and Infrasil[18]; 3) CHARMS Sellmeier fit for Homosil (VIS/NIR only); 4) CHARMS Sellmeier fit for Infrasil 301[19]; 5) a dispersion relation for Suprasil 3001 at room temperature obtained from an optical designer affiliated with the NISP team in the form of Schott index coefficients in a Zemax private glass library (derived through means unknown to us); and 6) CHARMS Sellmeier fit for Corning 7980.[20] In all cases other than for absolute measurements made in CHARMS, we first adjust catalog or library indices to vacuum by multiplying by the spectral index of refraction of air. Indices from CHARMS are then computed from our fit at 293 K (20 C) for comparison.

Note first, however, that the Suprasil family dispersion relation does not include Suprasil 3001, 3002, and we were unsuccessful obtaining a dispersion relation for the 3001 material explicitly from the manufacturer. We include Suprasil family here to illustrate that even within a product family name, there are still characteristic variations in index at the 0.1-0.2 ppt (part per thousand) level in index. The next thing we see is that our measurements of both Homosil and Infrasil 301 are in agreement with catalog values essentially to within our combined uncertainties (Heraeus rates accuracy in their dispersion relation at ±3E-5), but that the index of Suprasil 3001 is about 0.1 ppt higher than Homosil/Infrasil.

Likewise, the index of Suprasil 3001 is ~0.15-0.2 ppt higher in index than Corning 7980. Incidentally, we see that Corning 7980 and the Suprasil family (excluding 3001, 3002) have essentially the same catalog index relation. Finally, we observe that the CHARMS room temperature Sellmeier fit for Suprasil 3001 agrees with the NISP team's Zemax private library relation to within a few times our single measurement uncertainty. Thus, the NISP optical design team managed to get their hands on a quite sensible room temperature dispersion relation.

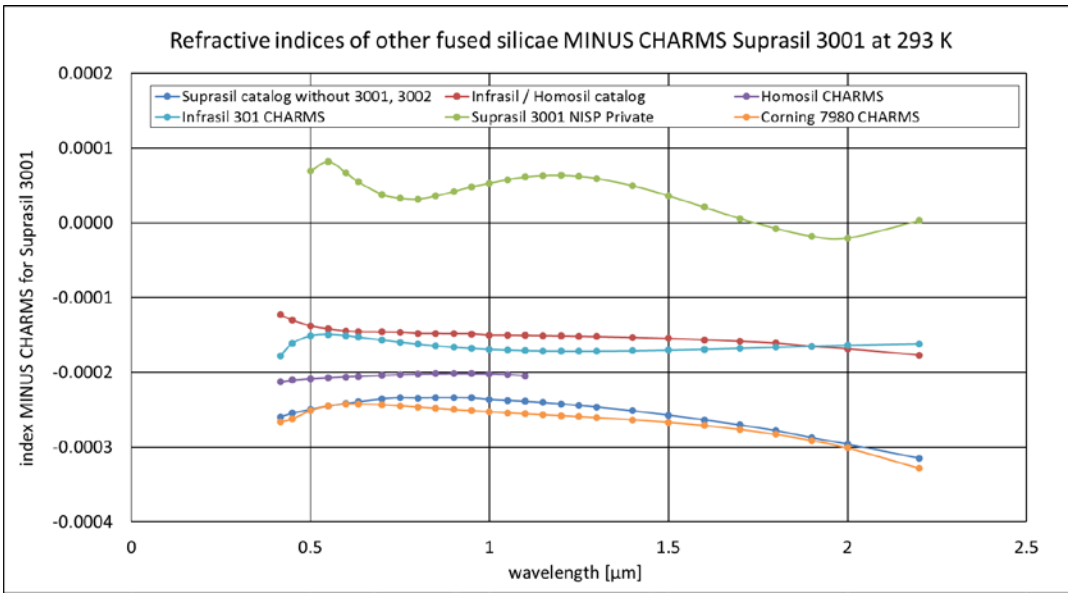

Figure 9 – comparison of various types of fused silica with Suprasil 3001 at room temperature in vacuum

5.2 S-FTM16

Prior to this study for NISP, we previously measured two different melts of S-FTM16 in CHARMS made at least 3 years apart and found that they differed in index by ~4E-4. The more recent c. 2006 melt measured for the design of the Keck MOSFIRE[21] instrument was found to be different from the glass manufacturer's catalog data[22] at room temperature by about +1.5E-4. This is not surprising since Ohara's specification for index variability in their glasses is ±5E-4. In Figure 10, we compare the CHARMS Sellmeier fit for NISP's two melts of S-FTM16 (that were the same in index to within our ability to discern) with the melt for MOSFIRE and with the room temperature catalog data. The melt for NISP is 5E-5 lower in index than the MOSFIRE S-FTM16 melt and about 1E-4 higher than the catalog index for S-FTM16.

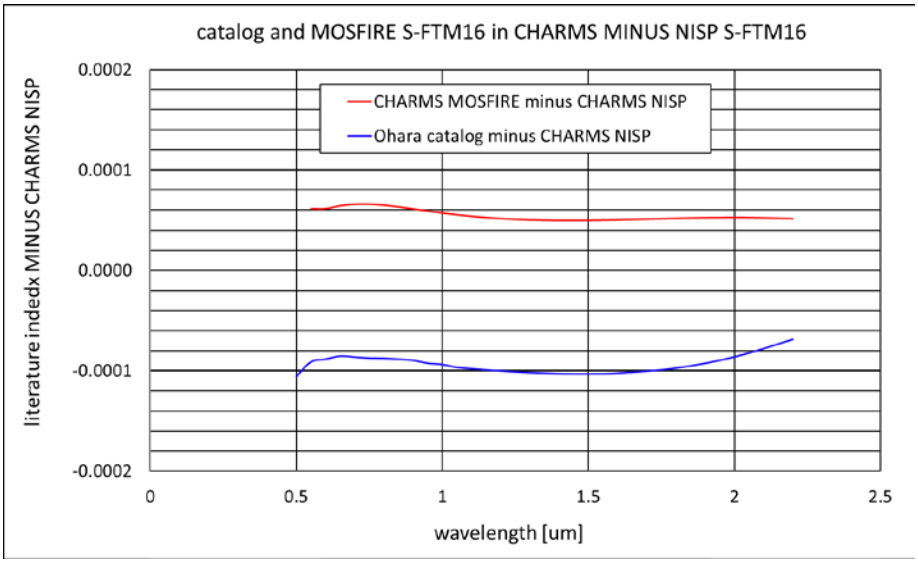

Figure 10 – comparison of a previous melt of S-FTM16 for MOSFIRE measured in CHARMS and catalog data at room temperature in vacuum with S-FTM16 for NISP measured in CHARMS

5.3 CaF_2

Since the mid-1990's, the refractive index of CaF_2 has been measured at cryogenic temperatures by several investigators including our group.[17,19,23] Since index measurements of CaF_2 with CHARMS are currently 3-5 times more accurate than and are based on more recently grown material than any of those other investigations, in Figure 11 we compare our Sellmeier fit for the three batches of CaF_2 for NISP with that from our own previous investigation for the ESO VLT X-shooter instrument.[8,19] The combined uncertainty for the two sets of measurements is ≥ 2E-5 for the wavelength range shown. Thus, to within our ability to tell, the absolute spectral index of the NISP CaF_2 is practically the same as that for X-shooter.

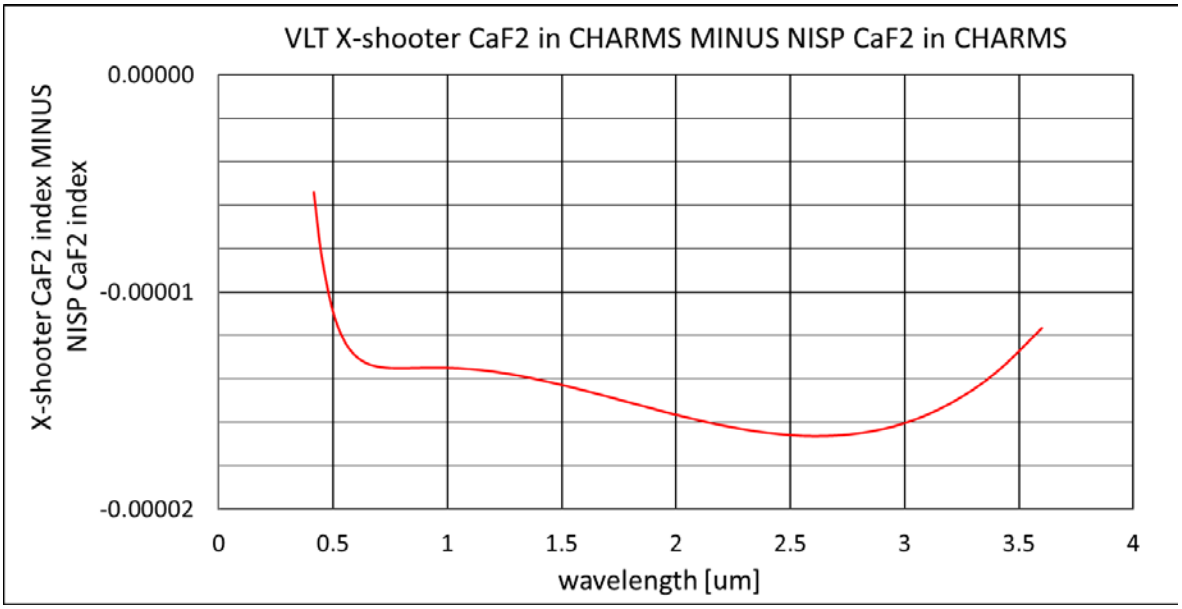

Figure 11 – comparison of absolute refractive index at room temperature of CaF_2 for NISP with batch of CaF_2 for ESO VLT X-shooter instrument, both measured in CHARMS

6. CONCLUSION

In support of the optical design and tolerancing of the Euclid Near Infrared Spectrometer and Photometer (NISP), we have measured the absolute refractive indices of two melts of Heraeus Suprasil 3001 fused silica for the first time from room temperature to cryogenic temperatures (110K) from the violet to 3.2 μm in the infrared and found them to be negligibly different from one another but different from other variants of synthetic fused silica by 2-3E-4 in index.

We also measured indices for two new melts of Ohara S-FTM16 glass from the violet to 2.72 μm at those same temperatures and found no practical difference in index between the two melts but differences of up to a few parts in the fourth decimal place of index between those and other melts of this glass we have measured previously.

Finally, we measured indices for three batches of CaF_2 from the violet to 3.56 μm from room temperature down to 100 K and found very slight but, we believe, real differences in index between the batches at the level of our single measurement index uncertainties. Treating the three batches as if they were one – using a single, temperature-dependent Sellmeier fit – we found that these batches were within our combined measurement uncertainties for previous batches we have measured at the 1.5E-5 level in index.

REFERENCES

[1] Leviton, D.B., Frey, B.J., "Design of a cryogenic, high accuracy, absolute prism refractometer for infrared through far ultraviolet optical materials," SPIE **4842**, 259 (2003), http://dx.doi.org/10.1117/12.459479
[2] Frey, B.J., Leviton, D.B., Henry, R.M., Quijada, M.A. "Cryogenic high-accuracy absolute prism refractometer for infrared through far-ultra-violet optical materials: implementation and initial results," SPIE **5172**, 119 (2003), http://dx.doi.org/10.1117/12.506097
[3] Leviton, D.B., Frey, B.J., "Cryogenic, High-Accuracy, Refraction Measuring System – a new facility for cryogenic infrared through far-ultraviolet refractive index measurements," SPIE **5494,** 492 (2004), http://dx.doi.org/10.1117/12.563795
[4] Leviton, D.B., Frey, B.J., Kvamme, T., "High accuracy, absolute, cryogenic refractive index measurements of infrared lens materials for JWST NIRCam using CHARMS," SPIE **5904**, (2005), http://dx.doi.org/10.1117/12.619306
[5] McLean, I.S., et al, "Design and development of MOSFIRE: the multi-object spectrometer for infrared exploration at the Keck Observatory," SPIE **7735**, (2010), http://dx.doi.org/10.1117/12.856715
[6] Kerber, F., Frey, B.J., Leviton, D.B., Bristow, P., Kaufl, H.U., Pirard, J., Rosa, M.R., "Calibration of the ZnSe pre-disperser on ESO's cryogenic IR echelle spectrograph (CRIRES): comparison of the first results from CRIRES and the laboratory data from CHARMS," SPIE **6269**-, (2006), http://dx.doi.org/10.1117/12.670393
[7] Sharples, R., et al, "Design of the KMOS multi-object integral-field spectrograph," SPIE **6269**, (2006), http://dx.doi.org/10.1117/12.669781
[8] Navarro, R., Elswijk, E., Tromp, N., Ter Horst, R., Horrobin, M., Vernet, J., Finger, G., Groot, P., Kaper, L., "X-shooter Near-IR Spectrograph Arm Realisation," SPIE **7014**, (2008); http://dx.doi.org/10.1117/12.789778
[9] Fabricant, D., et al, " NIRMOS: a wide-field near-infrared spectrograph for the Giant Magellan Telescope," SPIE **8446**, (2012), http://dx.doi.org/10.1117/12.926262
[10] Grupp, F., Prieto, E., Geis, N., Bode, A., Katterloher, R., Bodendorf, C., Penka, D., Bender, R., "The EUCLID NISP tolerancing concept and results," SPIE **9143**, (2014), http://dx.doi.org/10.1117/12.2055398
[11] Grupp, F.D., Leviton, D.B., Miller, K.H., Quijada, M.A., "The need for accurate cryo refractive indices and mechanical properties of optical materials (Lithosil 3001, CaF2 and S-FTM16 for EUCLID NISP)," SPIE, San Diego, (2015)
[12] Ricker, G.R., Winn, J.N., Vanderspek, R., Latham, D.W., Bakos, G.A, et al., "Transiting Exoplanet Survey Satellite", J. Astron. Telesc. Instrum. Syst. 1(1), 014003 (Oct 24, 2014), http://dx.doi.org/10.1117/1.JATIS.1.1.014003
[13] Pasquale, B., et al, "Optical Design of the WFIRST-AFTA Wide-Field Instrument," SPIE **9293**, (2014), http://dx.doi.org/10.1117/12.2177847
[14] Groff, T.D., et al, "Construction and status of the CHARIS high contrast imaging spectrograph," SPIE **9147**, 91471W, (2014), http://dx.doi.org/10.1117/12.2055769
[15] Groff, T.D., et al, "The CHARIS IFS for High Contrast Imaging at Subaru," SPIE, San Diego, (2015)
[16] Frey, B.J., Leviton, D.B., "Automation, operation, and data analysis in the cryogenic, high accuracy, refraction measuring system (CHARMS)," Proc. SPIE, **5904**, 59040P (2005), http://dx.doi.org/10.1117/12.619302
[17] Tropf, W.J., "Temperature-dependent refractive index models for BaF2, CaF2, MgF2, SrF2, LiF, NaF, KCl, ZnS, and ZnSe," Optical Engineering, **34**(5), 1369, May 1995, http://dx.doi.org/10.1117/12.201666
[18] Heraeus, http://www.heraeus-quarzglas.com
[19] Leviton, D.B., Frey, B.J., Madison, B.J., "Temperature-dependent refractive index of CaF2 and Infrasil 301," SPIE **6692**, (2007), http://dx.doi.org/10.1117/12.735594
[20] Leviton, D.B., Frey, B.J., "Temperature-dependent absolute refractive index measurements of synthetic fused silica," SPIE **6273**, (2006), http://dx.doi.org/10.1117/12.672853
[21] Leviton, D.B., Frey, B.J., Henry, R.M., "Temperature-dependent refractive index measurements of S-FPL51, S-FTM16, and S-TIM28 to cryogenic temperatures," SPIE **8863**, (2013), http://dx.doi.org/10.1117/12.2024821
[22] Ohara Optical Glass Catalog, http://www.oharacorp.com/
[23] Yamamuro, T., et al, "Measurement of refractive indices of 20 optical materials at low temperatures," Optical Engineering, **45**(8), (2006), http://dx.doi.org/10.1117/1.2336241